K. Karpinska [1][*], S. P. Malinowski[1]

[1] Institute of Geophysics, Faculty of Physics, University of Warsaw, Warsaw, Poland

1   INTRODUCTION

Recent studies attribute the evolution of droplet size distribution in warm convective clouds to enhancement of collision-coalescence by turbulence (see e.g. Devenish et al. (2012), Shaw (2003)). One of the influences turbulence has on droplets collision-coalescence is its effect on droplet positions leading to their uneven distribution in space. The aim of this study is a better understanding of the preferenial concentration of droplets from analytical and numerical analysis of droplet motion in vortex tubes: small coherent structures characteristic for high Reynolds number turbulent flows. Former research of such effects by Hill (Hill, 2005) and by Markowicz (Markowicz et al., 2000) was limited to horizontally oriented vortex tubes only. Herein we analyse tubes which are parallel or oblique to the direction of gravity.

2   VORTEX TUBE MODEL

Line vortex is a theoretical model of 3d structure of constant circulation (Γ) and singular vorticity concentrated on a straight line. In cylindrical coordinates (r, ϕ, z) in which vortex singularity lies on Z axis, its vorticity is given by:

$$\vec{\omega} = L_w \frac{\delta(r)}{r} \hat{e_z} \qquad (1)$$

while $L_w = \frac{\Gamma}{2\pi}$ is a parameter of vortex circulation. We use constant velocity field generated by line vortex with stretching of strenght $\gamma \left[\frac{1}{s}\right]$ as a model of vortex tube:

$$\vec{v_a} = -\frac{\gamma}{2} r \hat{e_r} + \frac{L_w}{r} \hat{e_\phi} + \gamma z \hat{e_z} \qquad (2)$$

Numerical simulations were done for visualization purposes with parameters corresponding to cloud/water droplets in an airflow. Two sets of vortex parameters were chosen for numerical simulations:

- strong vortex: $\gamma = 30 \frac{1}{s}$, $L_w = 0.025 \frac{m^2}{s}$,

[*]Corresponding author: Pasteura 7, 02–093 Warsaw, Poland, e–mail: karpinska@igf.fuw.edu.pl

- weak vortex: $\gamma = 0.5 \frac{1}{s}$, $L_w = 2.5 \cdot 10^{-4} \frac{m^2}{s}$.

Values of other parameters used were as follows: air kinematic viscosity $\mu = 1.776 \cdot 10^{-5} \frac{kg}{ms}$, water density $\rho_w = 1000 \frac{kg}{m^3}$, gravity of Earth $g = 9,81 \frac{m}{s^2}$.

We arranged our vortex model to cover all possible orientations with respect to gravity direction by introducing an angle $\theta \in [0, \pi]$ between gravity vector and vortex axis (see Figure 1):

$$\vec{g} = -g(\sin\theta \hat{e_y} + \cos\theta \hat{e_z})$$
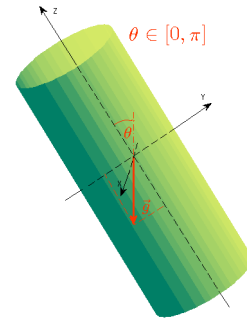
Figure 1: Scheme of gravity vector orientation in respect to the vortex axis

3   EQUATIONS GOVERNING DROPLET MOTION

We assumed that droplet is a point particle and its motion in fluid is determined by viscosity and gravity forces only, so no other hydrodynamical forces and no interaction with other droplets were included. Stokes equation with gravity was used as droplet equation of motion. In a fluid flow with velocity field v_a, for a droplet of mass m in a position $\vec{r}$ with inertial response time τ and under gravity force $F_g = m\vec{g}$ this equation is expressed by:

$$m\ddot{\vec{r}} = \frac{1}{\tau} m(\vec{v_a} - \dot{\vec{r}}) + m\vec{g}. \qquad (3)$$

Equation (3) was nondimensionalized with use of τ as time scale and length scale $S = \sqrt{L_w \tau}$ connected

to vortex circulation. The resulting equations of motion in a plane perpendicular to the vortex axis (here in (r, ϕ) coordinates) separate from motion along Z axis.

$$\begin{cases} \ddot{r} - r\dot{\phi}^2 = -(\frac{K_1}{2}r + \dot{r} + K_3 sin(\phi)) \\ 2\dot{r}\dot{\phi} + r\ddot{\phi} = \frac{1}{r} - r\dot{\phi} - K_3 cos(\phi)) \\ \ddot{z} = K_1 z - \dot{z} - K_2 \end{cases} \quad . \quad (4)$$

Motion of a droplet in case of gravity parallel to the vortex axis ($\theta = 0$) depends on two following dimensionless parameters:

$$\begin{aligned} L_1 &= \gamma\tau, \\ L_2 &= \frac{g\tau^2}{S}. \end{aligned} \quad (5)$$

and on three in case with gravity direction nonparallel to the vortex axis ($\theta \neq 0$):

$$\begin{aligned} K_1 &= \gamma\tau = L_1, \\ K_2 &= \frac{g\tau^2}{S}cos\theta = L_2 cos\theta, \\ K_3 &= \frac{g\tau^2}{S}sin\theta = L_2 sin\theta. \end{aligned} \quad (6)$$

L_2 parameter has a direct physical interpretation as a rate of droplet terminal velocity ($g\tau$) to characteristic velocity ($\frac{S}{\tau}$) and it determines whether motion of droplet is mainly gravitational or circular. L_2 is independent of vortex stretching, whereas L_1 express rate of velocity increment due to stretching at droplet characteristic length (γS) to the droplet characteristic velocity ($\frac{S}{\tau}$). K_2 and K_3 parameters has obviously the same interpretation as L_2, but their impact on solutions change with θ angle.

4 DROPLET DYNAMICS AROUND LINE VORTEX

We described droplet motion in general by analytical calculations and also by numerical simulations in cases of weak vortex and strong vortex.

4.1 Motion in direction parallel to the vortex axis

The third equation in (4) was solved with initial conditions $z(0) = z_0$, $\dot{z}(0) = 0$. The following formula describes motion of droplet along Z axis (vortex axis):

$$z(t) = \frac{z_0 - z_{0b}}{\lambda_+ - \lambda_-}\left[\lambda_+ exp(\lambda_- t) - \lambda_- exp(\lambda_+ t)\right] + z_{0b},$$
$$(7)$$

$$\lambda = \lambda(K_1), \quad \lambda_+ > 0, \quad \lambda_- < 0 \quad (8)$$

while $z_{0b} = \frac{K_2}{K_1}S$.

Direction of motion along Z axis is therefore determined only by the initial position of droplet z_0. If $z_0 = z_{0b}$ ($z_{0b} > 0$) the droplet stays in unstable steady position in respect to this motion. Stable position is proportional to second power of droplet radius and decreases with growing θ angle and stretching strenght: $z_{0b} \propto \gamma^{-1}R^2\cos\theta$ so for droplets of different sizes their stable positions get closer to each other with growing θ and γ. If $z_0 > z_{0b}$ or $z_0 < z_{0b}$ droplet moves nearly exponentially up or down respectively along the vortex axis. Its linear acceleration equals $-g\cos\theta$ at the start, then decrease due to viscosity force and then rapidly increase due to vortex stretching.

These formula and conclusions are valid for the whole range of angles $\theta \in [0, \frac{\pi}{2}]$. In a special case of $\theta = 0$ general parameters of motion K_1, K_2 become already mentioned L_1, L_2 parameters.

4.2 Motion in plane perpendicular to the vortex axis

Motion in a plane perpendicular to the vortex axis shows strong qualitative dependence on angle θ. For this reason cases of "vertical vortex", meaning $\theta = 0$ and "oblique vortex" with $\theta \neq 0$ are analysed separately.

4.2.1 Line vortex parallel to gravity

In this case there is only one kind of solution for motion in plane (r, ϕ): every droplet has its circular stable, periodic orbit on which radial viscous force and centrifugal force equalize. Radius of this orbit is $r_{orb} = \sqrt[4]{\frac{2\tau}{\gamma}(\frac{\Gamma}{2\pi})^2}$ so it increase with increasing vortex circulation and droplet radius as well as with decreasing stretching strength. Stability of the orbit guarantees that trajectories of all the droplets spirals into it in finite time. Angular velocity of initially stationary droplets very quickly increases and decreases at the beginning of the simulation and later tends to smaller, constant value of $\dot{\phi}_{orb} = \sqrt{\frac{\gamma}{2\tau}}$.

Figure 2 presents a 3d droplet trajectory with initial position $r_0 > r_{orb}, z_0 < z_{0b}$ and initial zero velocity. If time that droplet needs to get on its 2d steady orbit is small in comparison with timescale of motion along Z axis than it can reside on its 3d orbit for significant amount of time.

Numerical simulations for 3d droplet motion in the weak vortex for radii range $1 - 20\mu m$ gave the following results:

- There is significant difference of "'residence time'" of small and large particles: time of getting on the steady orbit for small droplets is very short in comparison to characteristic time of vertical fall (or lifting) resulting in the effect of long stay of small droplets on their circular, steady, periodic orbits.

2
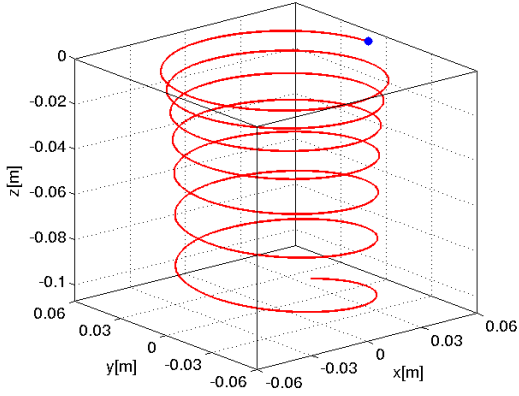
Figure 2: Trajectory of droplet of radius $R = 10\mu m$ in weak vortex with initial position $r_0 > r_{orb}$, $z_0 < z_{0b}$ in time $t \in [0, 10s]$.

- Trajectories of droplets in the same initial position but different initial velocities (zero and fluid velocity) show strong dependence on this initial condition, which can be described as a sling effect (Falkovich and Pumir, 2007).

4.2.2 Line vortex nonparallel to gravity

Gravity influence destroys axial symmetry of motion in a plane perpendicular to the vortex axis. It manifests in the equations by additional K_3 parameter dependence. In consequence solution of equations in a form of round, stable, periodic orbit does not exist for any droplet in this case. Gravity influence on motion results however in possibility of apperance of equillibrium points in the IV quadrant of the plane described with (x,y) coordinates. Positions of these points described in (r, ϕ) are as follows:

$$r_{st\pm} = \sqrt{2}\frac{K_3}{K_1}\sqrt{1 \pm \sqrt{1 - \frac{K_1^2}{K_3^2}}}$$
$$\phi_{st\pm} = -arcsin(\frac{1}{\sqrt{2}}\sqrt{1 \pm \sqrt{1 - \frac{K_1^2}{K_3^2}}}) \quad (9)$$

under the condition $K_3^2 \geq K_1$. This condition splits into two:

$$L_2^2 \geq L_1,$$
$$\theta \in (arcsin(\sqrt{\frac{L_1}{L_2^2}}), \frac{\pi}{2}). \quad (10)$$

The existence condition was pictured in Figure 3: for given vortex of γ and L_w equillibrium point may exist only for droplets of radii above the drawn surface. Droplets which fulfill the first part of condition
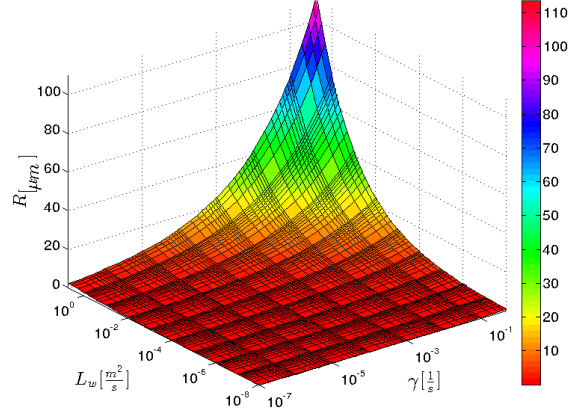
Figure 3: Boundary surface presenting equillibrium points existence condition for a range of droplets reaching 100 μm.

(10) with equality (are positioned on the surface plotted in Figure ??) for a given γ and L_w can have an eqillibrium point only when the vortex axis is perpendicular to gravity vector, $\theta = 0$. For example the boundary droplet radius stemming from above condition for strong vortex is $84.07 \ \mu m$, for weak vortex it is $9.56 \ \mu m$.

Linear stability of the two solutions for equillibrium points (see equation (9)) was examined (as in Marcu et al. (1995)) for the case of Burgers vortex) and the conclusions are as follows:

- r_{st-} is always unstable,

- r_{st+} is unstable only under conditions: $K_1 \in (\frac{1}{4}, \frac{1}{2})$ and $K_3^2 \leq \frac{K_1^2 - \frac{1}{2}K_1 + \frac{1}{8}}{\frac{1}{2} - K_1}$.

Numerical simulations show also apperance of noncircular limit cycle under certain vortex/droplet conditions. It can be a unique stable solution or compete with the stable eqillibrium point. Generally the result of leaning the line vortex with respect to gravity leads to droplet 2d motion in which it approaches one of two types of attractors: either a stable limit cycle or a stable equillibrium point. Figure 4 presents examples of trajectories of same-sized droplets in the weak and the strong vortices accordingly in which we can see the situation of coexistence of noncircular stable limit cycle with stable eqillibrium point.

In the weak vortex we observe significant influence of gravity on motion of droplets only for those of radii close to boundary radius. For smaller droplets there are stable limit cycles of shape close to circular. For bigger droplets, as in Figure 4a) fast approaching the limit cycle was observed with its shape slightly deviated from circular in closeness of stationary point.

3
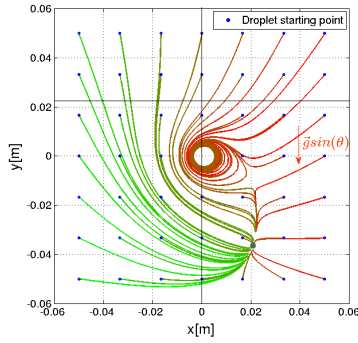
(a) $R = 10 \ \mu m$, weak vortex
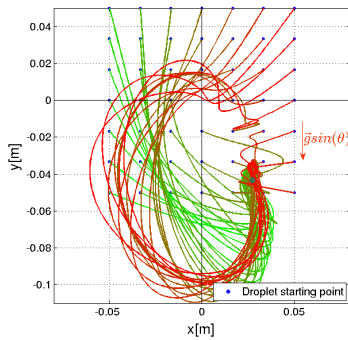
(b) $R = 85 \ \mu m$, strong vortex

Figure 4: Trajectories of 36 droplets seen in XY cross-section of radius R distributed uniformly in a plane $z = 0$ on a rectangle l=8cm in a vortex with $\theta = 0.45\pi$.

In the strong vortex however this influence is easily seen even for droplets much smaller than boundary radius. The shape of trajectories generally is very complicated, there are also great fluctuations of velocity while attracted by the stable limit cycle. This is shown for droplets of radius close to boundary in Figure 4b).

4.3 Various size droplets motion simulations

Figures 5 and 7 are frames from 3d simulations of motion of various size droplets in the weak and in the strong vortex. They are cross-sections perdpendicular to the vortex axis while Figure 6 is a projection of 3d picture of the same visualization for weak vortex. Red and orange lines are plots of equilibrium points positions for those droplets from a chosen range for which they exist. The overlaying of these lines by endpoints of trajectories of droplets is a visualization for good agreement between analytical and numerical results.

Different types of droplets behaviour (periodic orbits, limit cycles, equilibrium points) described above strongly influence space distribution of different size droplets as seen in Figures 5, 7 and 6. This effect is strong especially if the timescale of motion along the vortex axis is increased by vortex leaning. Figure 6 indicates that in oblique, line vortex droplets of various radii tend to separate in space. Smaller droplets are attracted by their periodic orbits around the vortex axis while motion of the bigger ones is determined more by gravity and equillibrium point attraction.

5 CONCLUSIONS

Features such as stable periodic orbits, stable eqillibrium points and limit cycles were identified qualitatively as three-dimensional structures that may lead to enhancement of preferential concentration of droplets in clouds. Conditions for existence of periodic orbits and equillibrium points were derived as well as their stability was verified. Numerical solutions agree with analytical results.

Acknowledgements

References

Devenish, B. J., and Coauthors, 2012: Review article. droplet growth in warm turbulent clouds. *Q. J. R. Meteorol. Soc.*, **138**, 1401–1429, doi:10.1002/qj.1897.

Falkovich, G., and A. Pumir, 2007: Sling effect in collisions of water droplets in turbulent clouds. *J. Atmos. Sci.*, **64**, 4497–4505, doi:10.1175/2007JAS2371.1.

Hill, R. J., 2005: Geometric collision rates and trajectories of cloud droplets falling into a burgers vortex. *Phys. Fluids*, **17**, 037 103, doi:10.1063/1.1858191.

Marcu, B., E. Meiburg, and P. K. Newton, 1995: Dynamics of heavy particles in a burgers vortex. *Phys. Fluids*, **7**, 400–410, doi:10.1063/1.868778.

Markowicz, K. P., K. Bajer, and S. P. Malinowski, 2000: Influence of the small-scale turbulence structure on the concentration of cloud droplets. *Proc. of 13th Conf. on Clouds and Precip., IAMAP*.

Shaw, R. A., 2003: Particle-turbulence interactions in atmospheric clouds. *Annu. Rev. Fluid Mech.*, **35**, 183–227, doi:10.1146/annurev.fluid.35.101101.161125.

(a) t=0s

(b) t=1s
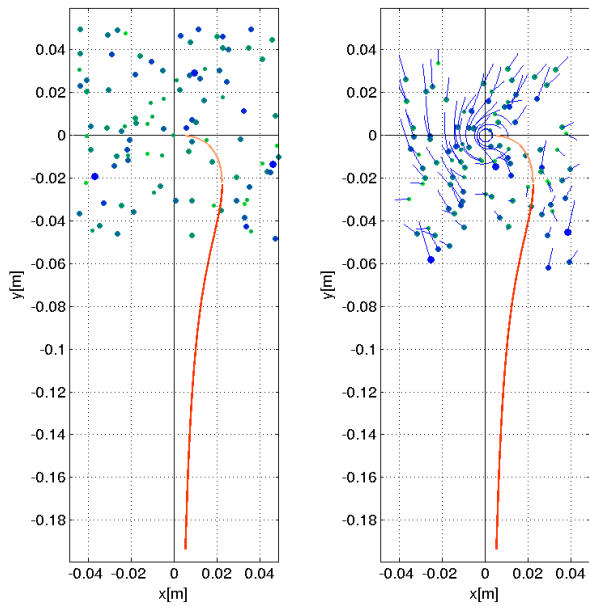
Figure 6: Positions of 100 droplets of various radius from range [1, 20 μm] starting in a plane $z = 0$ on a rectangle l=8cm, in the weak vortex with $\theta = 0.45\pi$ in t=4.5 s.
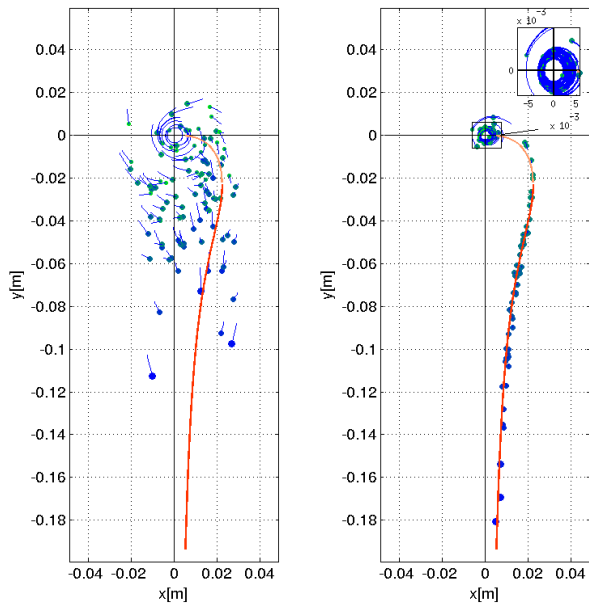
(c) t=3.2s

(d) t=15s

Figure 5: Positions of 100 droplets seen in XY crosssection of various radius from range [1, 20 μm] starting in a plane $z = 0$ on a rectangle l=8cm, in the weak vortex with $\theta = 0.45\pi$.
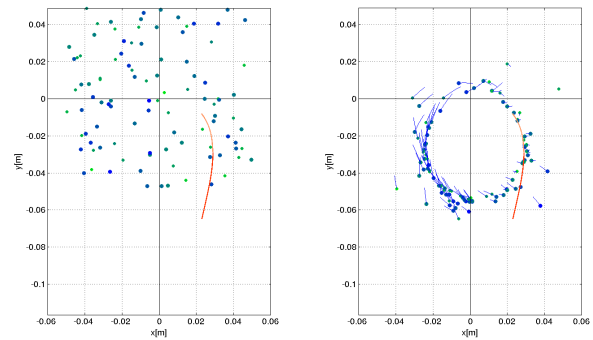
(a) t=0s

(b) t=0.1s
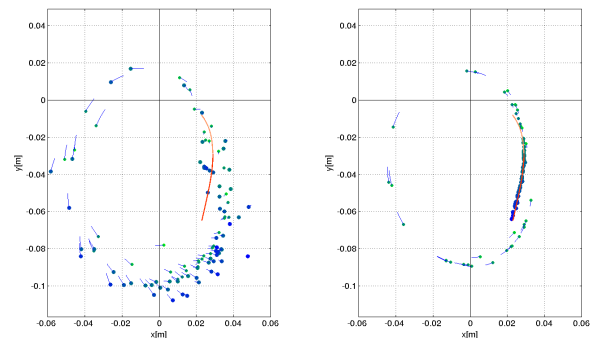
(c) t=0.2s

(d) t=1s

Figure 7: Positions of 100 droplets seen in XY crossection of various radius from range [75, 95 μm] starting in a plane $z = 0$ on a rectangle l=8cm, in the strong vortex with $\theta = 0.45\pi$.

5